PLOS | ONE

RESEARCH ARTICLE

Surface Reconstruction from Parallel Curves with Application to Parietal Bone Fracture Reconstruction

Abdul Majeed[1]*, **Abd Rahni Mt Piah**[2], **Zainor Ridzuan Yahya**[3]

1 Division of Science and Technology, University of Education, Town Ship Lahore, Pakistan, **2** School of Mathematical Sciences, Universiti Sains Malaysia, 11800 Penang, Malaysia, **3** Institute of Engineering Mathematics, Universiti Malaysia Perlis, Pauh Putra Campus, 02600 Pauh, Perlis, Malaysia

* abdulmajeed@ue.edu.pk

Citation: Majeed A, Mt Piah AR, Ridzuan Yahya Z (2016) Surface Reconstruction from Parallel Curves with Application to Parietal Bone Fracture Reconstruction. PLoS ONE 11(3): e0149921. doi:10.1371/journal.pone.0149921

Editor: Jose Manuel Garcia Aznar, University of Zaragoza, SPAIN

Received: September 1, 2015

Accepted: February 6, 2016

Published: March 11, 2016

Data Availability Statement: The authors obtained DICOM data from Universiti Sains Malaysia (USM) health campus with the approval of Human Research Ethic Committee (USM). The letter of this committee has been attached. Ethically the authors cannot provide the data directly to any researcher as the data is a real patient data; however, interested researchers can contact the School of Dental Sciences (USM) to place a request (jepem@kk.usm.my).

Funding: The authors would like to extend their gratitude to the Ministry of Education of Malaysia and Universiti Sains Malaysia for supporting this work

Abstract

Maxillofacial trauma are common, secondary to road traffic accident, sports injury, falls and require sophisticated radiological imaging to precisely diagnose. A direct surgical reconstruction is complex and require clinical expertise. Bio-modelling helps in reconstructing surface model from 2D contours. In this manuscript we have constructed the 3D surface using 2D Computerized Tomography (CT) scan contours. The fracture part of the cranial vault are reconstructed using GC^1 rational cubic Ball curve with three free parameters, later the 2D contours are flipped into 3D with equidistant z component. The constructed surface is represented by contours blending interpolant. At the end of this manuscript a case report of parietal bone fracture is also illustrated by employing this method with a Graphical User Interface (GUI) illustration.

Introduction

Craniofacial region is a complex anatomical part made up of various bones joined together. Fig 1 illustrates the various bones that make up the human skull. Craniofacial fractures occurs due to various etiological factors like road traffic accident (RTA), sports injury falls etc. Various diagnostic tools like X rays, Computerized Tomography (CT) scans, Magnetic Resonance Image (MRI) have been used to diagnose the craniofacial fractures. Since, craniofacial fractures do not follow a specific pattern and lately, emerging virtual reconstruction technologies opened new avenues for mathematicians, physicists and software engineers to reconstruct the fracture defects. Already established approaches for implant design is Computer Aided Design (CAD)/Computer Aided Manufacturing (CAM) process chain [1]. Other alternative methods that design implant without CAD process are mirroring [2] and surface interpolation also called as deformation [3].

The methods used for the construction of fracture segment are either anatomical or mathematical features. The mirroring method is useful for the fracture on one side of the skull only and use anatomical features. While mathematical constraints are used in interpolation and

under its Fundamental Research Grant Scheme (FRGS), Account No. 203/PMATHS/6711365. The funders had no role in study design, data collection and analysis, decision to publish, or preparation of the manuscript.

Competing Interests: The authors have declared that no competing interests exist.

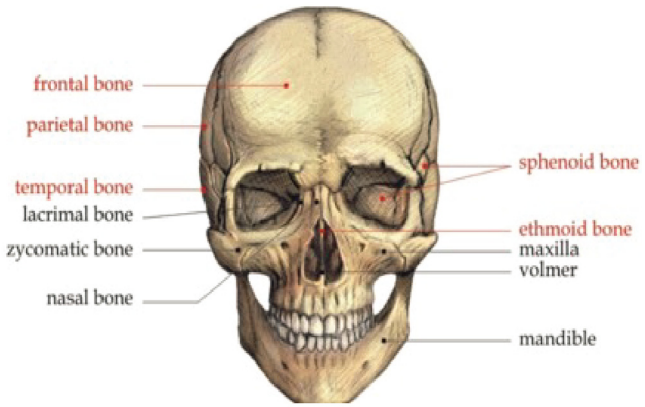

Fig 1. Craniofacial bones.

doi:10.1371/journal.pone.0149921.g001

deformation methods to construct the fractured part from the non fractured part of skull. Reference model is also used to construct the fractured part of skull [4]. For more related work (see [5–23] and references therein).

Contours blending function have been used to construct the 3D parietal bone fracture. Since Digital Imaging and Communications in Medicine (DICOM) data used in our work are in 2D form, so, before constructing the 3D surface, firstly, we have constructed fracture part curves using geometric continuity (GC^1) rational cubic Ball curves with three free parameters. Genetic Algorithm (GA) is used to optimize the free parameters. Then, we converted the 2D contour curves in 3D form by taking equidistant z component and then construct the 3D parietal bone fracture.

We present a case report of parietal bone fracture to show the applicability of proposed algorithm. The Dicom data are obtained from Hospital Universiti Sains Malaysia (HUSM). We employed matlab for both the programming and to develop Graphical User Interface (GUI) for parietal bone fracture reconstruction using proposed algorithm. Surgeons can use GUI for fracture reconstruction without having in depth knowledge of its mathematical aspect.

The introduction is followed by the representation of Ball basis functions and rational cubic Ball curve. It is followed by an explanation on contour blending, boundary extraction, parametrization, Normalized mean squares error. After this, we have explained the Graphical User Interface (GUI). An algorithm on 3D parietal bone fracture reconstruction using rational Ball curve and contour blending is proposed after the explanation of GUI.

Cubic Ball Basis Functions and Curve

The cubic Ball polynomial basis was first proposed by Ball [24] for CAD systems application. Fig 2 illustrates these functions against its parameter θ. The Ball basis functions can be written as

$$S_0(\theta) = (1-\theta)^2,\ \ S_1(\theta) = 2\theta(1-\theta)^2,$$
$$S_2(\theta) = 2\theta^2(1-\theta),\ \ S_3(\theta) = \theta^2. \tag{1}$$

Theorem 1: The Ball basis functions defined in Eq (1) have the following properties

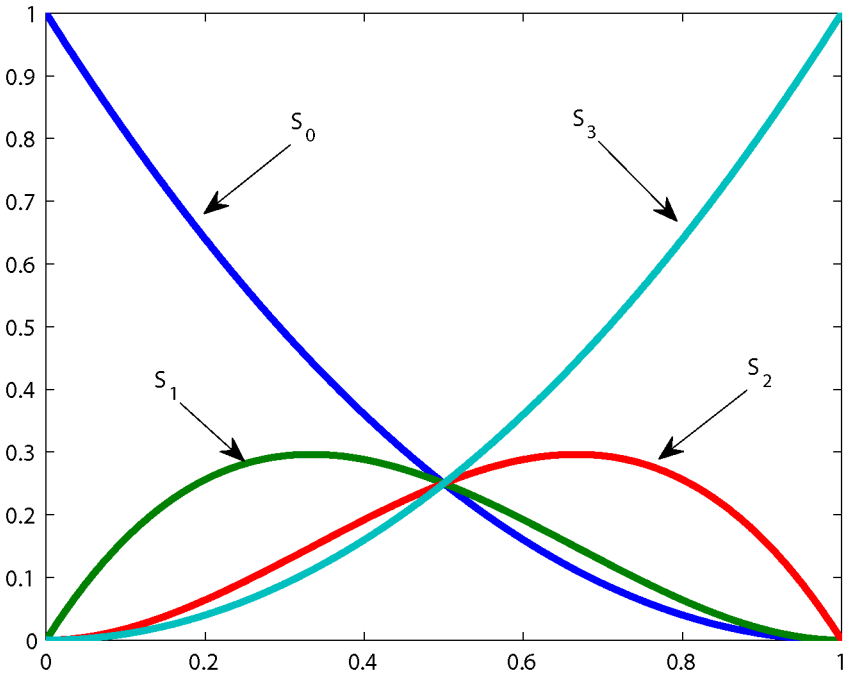

Fig 2. Ball basis functions.

doi:10.1371/journal.pone.0149921.g002

- Linearly Independent: The Ball basis functions are linearly independent. There do not exist set of non zero constants $a_0, \ldots, a_3$, for which.

$$\sum_{i=0}^{3} a_i S_i(\theta) = 0.$$

- Non Negative: Ball basis functions are non negative when $\theta \in [0, 1]$.
- Symmetric: The Ball basis functions are symmetric as

$$S_i(\theta) = S_{3-i}(1-\theta).$$

- Monotonicity: $S_0(\theta)$ is monotonically decreasing and $S_3(\theta)$ is monotonically increasing when $\theta \in [0, 1]$.
- Partition of Unity: Ball basis functions form a partition of unity, it means that sum of Ball basis functions will be 1.

$$\sum_{i=0}^{3} S_i(\theta) = 1.$$

Theorem 2: Let P_i be the set of control points and $S_i(\theta)$, $i = 0, \ldots, 3$ are Ball basis functions defined in Eq (1). The Ball curve $s(\theta) = \sum_{i=0}^{3} P_i S_i(\theta)$ have the following properties

- Coordinate system independence: As the Ball basis functions form partition of unity, so the Ball basis curve will be coordinate system independence. It means that by changing the coordinate system of control points curve will remain same.

- Convex Hull Property: As the Ball curve obeys the coordinate system independence and Ball basis functions are all non negative. So Ball curves will obey the convex hull property. It means that curves formed by Ball basis always lie within the convex hull of their control points.

$$\sum_{i=0}^{3} S_i(\theta) = 1, \quad S_i(\theta) \geq 0, \quad 0 \leq \theta \leq 1, \ i = 0, ..., 3.$$

- Variation Diminishing Property (VDP): Variation Dimension Property is obeyed by Ball curves. VDP is stated as if a curve is intercepted by straight line in b number of points and control polygon by p number of points, then it will always hold that

$$b = p - 2k$$

as shown in Fig 3. Where k is 0 or a positive integer.

- Endpoint Interpolation: The Ball curves always passes through the first and last control points.

$$s(0) = P_0, s(1) = P_3.$$

Theorem 3: Let P_i be the set of control points and $S_i(\theta)$, $i = 0, \ldots, 3$ are Ball basis functions defined in Eq (1). The Ball curve $s(\theta) = \sum_{i=0}^{3} P_i S_i(\theta)$ have the following distinctive advantages over Bezier basis curve

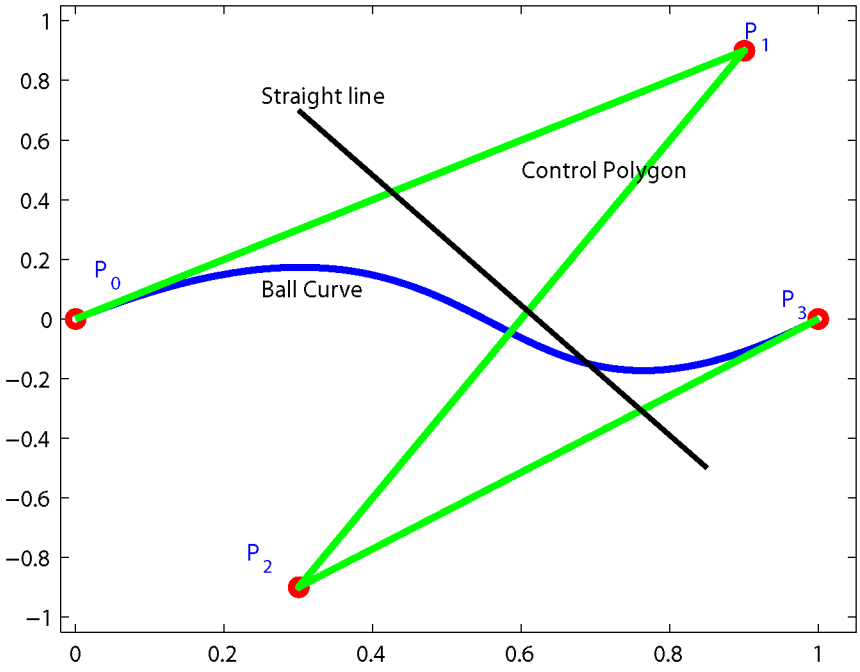

Fig 3. Variation diminishing property with b = 1 p = 3 k = 1.

doi:10.1371/journal.pone.0149921.g003

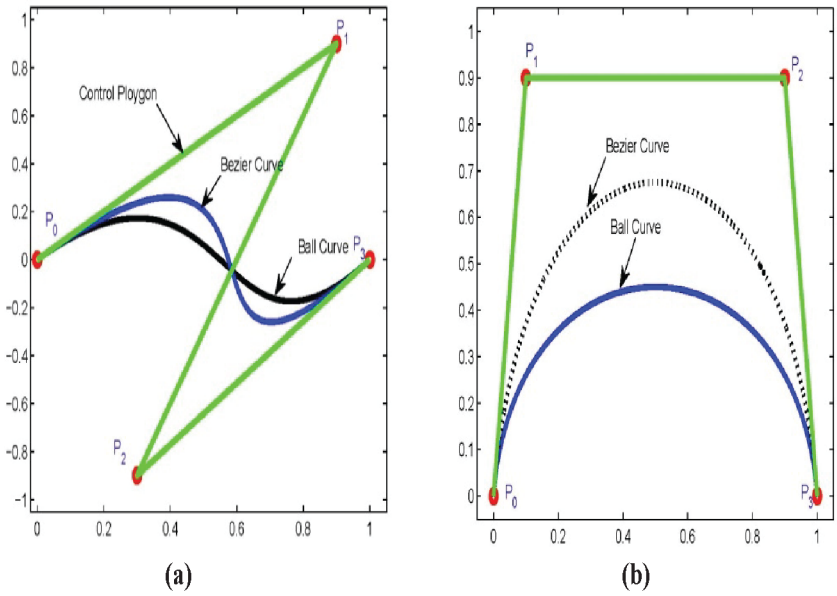

Fig 4. Ball verses Bezier curve.

doi:10.1371/journal.pone.0149921.g004

- The cubic Ball curve reduce to quadratic curve if $P_1 = P_2$.

$$s(\theta) = S_0(\theta)P_0 + 2S_1(\theta)P_1 + 2S_2(\theta)P_2 + S_3(\theta)P_3,$$
$$= (1-\theta)^2 P_0 + 2\theta(1-\theta)^2 P_1 + 2\theta^2(1-\theta)P_1 + \theta^2 P_3,$$
$$= (1-\theta)^2 P_0 + 2\theta(1-\theta)P_1 + \theta^2 P_3.$$

- The Ball curve passed away from the convex hull intermediate control points as compared to the Bezier curve as shown in Fig 4.
- Operation of degree elevation and reduction for a polynomial curve with Ball basis functions are simpler and faster than the curve with Bezier basis functions [25].

GC^1 Rational Cubic Ball Curve

The cubic rational Ball curve $s(\theta)$ defined in [26, 27] is

$$s(\theta) = \frac{P(\theta)}{Q(\theta)}, \quad 0 \le \theta \le 1, \tag{2}$$

where

$$P(\theta) = A(1-\theta)^2 + B(1-\theta)^2\theta + C(1-\theta)\theta^2 + D\theta^2,$$
$$Q(\theta) = (1-\theta)^2 + a(1-\theta)^2\theta + b(1-\theta)\theta^2 + \theta^2.$$

For GC^1 continuity consider the two consecutive curve segments

$$s_i(\theta) = \frac{P_i(\theta)}{Q_i(\theta)}, \quad i = 1, \ldots, n-1, \tag{3}$$

$$s_{i+1}(\theta) = \frac{P_{i+1}(\theta)}{Q_{i+1}(\theta)}, \quad i = 1, ..., n-1. \tag{4}$$

where

$$P_i(\theta) = A_i(1-\theta)^2 + B_i(1-\theta)^2\theta + C_i(1-\theta)\theta^2 + D_i\theta^2,$$

$$Q_i(\theta) = (1-\theta)^2 + a_i(1-\theta)^2\theta + b_i(1-\theta)\theta^2 + \theta^2,$$

$$P_{i+1}(\theta) = A_{i+1}(1-\theta)^2 + B_{i+1}(1-\theta)^2\theta + C_{i+1}(1-\theta)\theta^2 + D_{i+1}\theta^2,$$

$$Q_{i+1}(\theta) = (1-\theta)^2 + a_{i+1}(1-\theta)^2\theta + b_{i+1}(1-\theta)\theta^2 + \theta^2.$$

satisfying the following conditions

$$\begin{cases} s_i(0) = A_i, \ \ s_i(1) = D_i, \\ s_{i+1}(0) = A_{i+1}, \ \ s_{i+1}(1) = D_{i+1}, \\ s_i(1) = s_{i+1}(0), \\ s'_{i+1}(0) = \lambda_i s'_i(1). \end{cases} \tag{5}$$

using the above geometric continuity condition we can write

$$\begin{cases} s_i(0) = f_i = A_i, \ \ s_i(1) = f_{i+1}, \\ s_{i+1}(0) = f_{i+1}, \ \ s_{i+1}(1) = f_{i+2}, \\ D_i = A_{i+1} = f_{i+1}, \\ B_{i+1} = (a_{i+1} + \lambda_i b_i)f_{i+1} - \lambda_i C_i. \end{cases} \tag{6}$$

where f_i, f_{i+1}, f_{i+2} $i = 1, \ldots, n-1$ are the on curve control points and a_i, b_i and λ_i are free parameters. For curve fitting, firstly, we will find off curve control points using least square method. Then, free parameters will be optimized with the help of genetic algorithm.

In [28] the continuity between two curve segments is parametric continuity C^1 while in current work the continuity between two curve segments is geometric continuity GC^1 as the geometric continuity is more flexible than parametric. We have used C^1 rational Ball curves with tangents at end points. The tangent vectors work as intermediate control points, while in current work we are using GC^1 rational Ball curves and the intermediate control points are evaluated using least square method. In the current work the number of free parameters is increased to three and the proposed method is more flexible due to its geometric continuity. The proposed method works well for both small and large fractured parts. In current work we have extended the 2D CT scan data into 3D format taking equidistant z-component to construct the 3D craniofacial fractured part.

Effect of Control Point and Free Parameters

Ball curve can be changed or controlled by twofold. Firstly, by changing the off curve control points. For example in Fig 5, by changing the positron of P_1 control point the curve bend toward P_1. Similarly, with P_2 control point keeping the free parameters unchanged. Secondly, by changing the free parameter a and keeping b constant. For example in Fig 6, the curve bends toward P_1. Likewise, by changing b the curve will bend toward P_2.

The given Dicom data are in $2D$ form. To construct the surface, patch one have to convert the data in $3D$ form. For this, we took the non decreasing z component of each $2D$ contours as

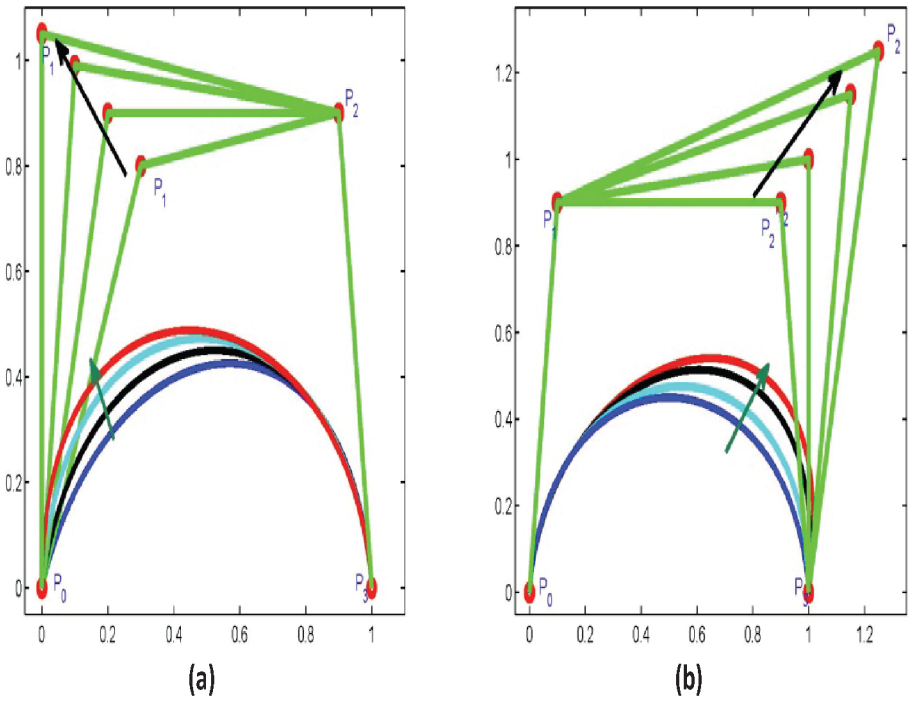

Fig 5. Effect of control points on curve.

doi:10.1371/journal.pone.0149921.g005

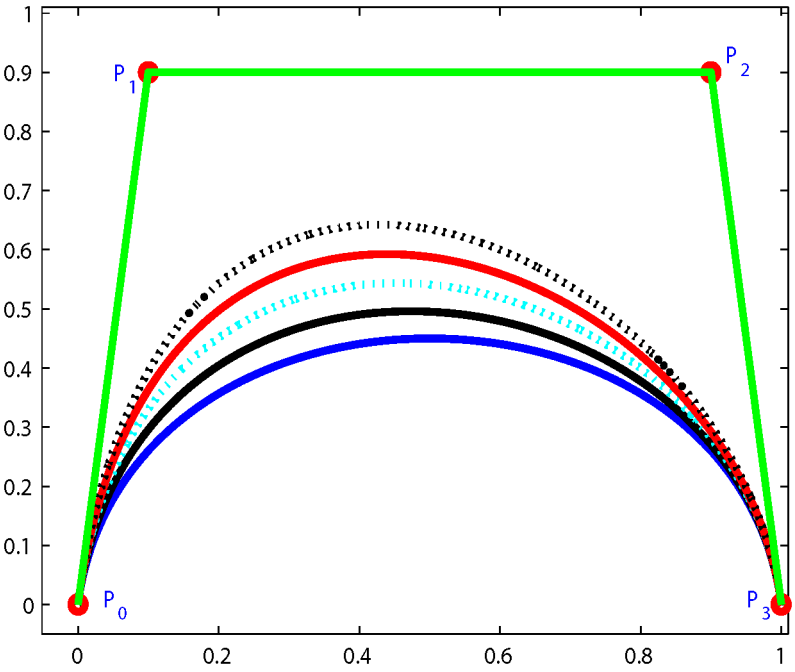

Fig 6. Effect of free parameters black curve when a = 1, b = 1 blue a = 1.4, b = 1 black a = 1.6, b = 1 cyan a = 1.8, b = 1 red a = 2, b = 1 black.

doi:10.1371/journal.pone.0149921.g006

a height like $z_0 < z_1 < \ldots < z_{max}$. The i^{th} contour is defined by the sequence of distinct data points which are counterclockwise ordered in the contour at the height z_i.

Contours Blending

The fracture part curves for each $2D$ contour have been constructed using proposed interpolant, and is converted into $3D$ form taking equidistant z component [29]. Let $C^{i-1}(\psi)$, $C^i(\psi)$ and $C^{i+1}(\psi)$ are missing part curves at height z^{i-1}, z^i and z^{i+1} respectively. The cubic Ball interpolant can be written as

$$B^i(\theta,\psi) = C^i(\psi)S_0(\theta) + (z^{i+1} - z^i)v^i(\psi)S_1(\theta) + v^{i+1}(\psi)S_2(\theta) + C^{i+1}(\psi)S_3(\theta), \quad (7)$$

for $i = 1, \ldots, n-1$, $0 \le \theta, \psi \le 1$,

where n represents the number of contours. S_j, $j = 0, \ldots, 3$. are Ball basis polynomial functions defined in Eq (1).

$v^i(\psi)$ is a tangent to surface at $(C^i(\psi), z^i)$, to define the tangent vector let

$P^i(\psi) = (C^i(\psi), z^i)$ for $i = 1, \ldots, n$. Where $P^i(\psi)$ is in 3D form because $C^i(\psi)$ is in $2D$ form. Let

$$\hat{V}_i(\psi) = |C^{i+1}(\psi) - C^i(\psi)|(P^i(\psi) - P^{i-1}(\psi)) + |C^i(\psi) - C^{i-1}(\psi)|(P^{i+1}(\psi) - P^i(\psi)).$$

Thus $\hat{V}_i(\psi)$ is a complex combination of the vector $(P^i(\psi) - P^{i-1}(\psi))$ and $(P^{i+1}(\psi) - P^i(\psi))$. The $z-$*component* of $\hat{V}_i(\psi)$ is

$|C^{i+1}(\psi) - C^i(\psi)|(z^i - z^{i-1}) + |C^i(\psi) - C^{i-1}(\psi)|(z^{i+1} - z^i)$. Let $V_i(\psi)$ be the vector product when $\hat{V}_i(\psi)$ is divided by its $z-$*component*.

Then $V_i(\psi) = (v^i(\psi), 1)$ where

$$v^i(\psi) = \frac{|C^{i+1}(\psi) - C^i(\psi)|(C^i(\psi) - C^{i-1}(\psi)) + |C^i(\psi) - C^{i-1}(\psi)|(C^{i+1}(\psi) - C^i(\psi))}{|C^{i+1}(\psi) - C^i(\psi)|(z^i - z^{i-1}) + |C^i(\psi) - C^{i-1}(\psi)|(z^{i+1} - z^i)}.$$

$$v^i(\psi) = \frac{|D_1|D_2 + |D_2|D_1}{D_1(z^i - z^{i-1}) + D_2(z^{i+1} - z^i)}$$

where $D_1 = C^{i+1}(\psi) - C^i(\psi)$ and $D_2 = C^i(\psi) - C^{i-1}(\psi)$.

The vector $V_i(\psi)$ will be chosen to be a tangent to the surface at $P^i(\psi)$. If $C^{i+1}(\psi) = C^i(\psi) = C^{i-1}(\psi)$, then $D_1 = D_2 = 0$ and $v^i(\psi)$ is set to be $(0, 0)$.

As $v_i(\psi)$ lies in a plane containing $P^{i+1}(\psi)$, $P^i(\psi)$ and $P^{i-1}(\psi)$. If these points lie in a vertical plane, then

$$C^{i+1}(\psi) - C^i(\psi) = \lambda v^*(\psi)$$

$$C^i(\psi) - C^{i-1}(\psi) = \mu v^*(\psi)$$

for some unit vector $v^*(\psi)$ and some scalers λ and μ. Then

$$v^i(\psi) = \frac{|\mu|\lambda + |\lambda|\mu}{|\mu|(z^{i+1} - z^i) + |\lambda|(z^i - z^{i-1})} v^*(\psi)$$

If $\lambda\mu < 0$, then $|\mu|\lambda = -|\lambda|\mu$ and $v^i(\psi) = 0$.

If $\lambda\mu > 0$, then

$$v^i(\psi) = \frac{2\mu\lambda}{\mu(z^{i+1} - z^i) + \lambda(z^i - z^{i-1})} v^*(\psi)$$

Dividing denominator and numerator by $(z^{i+1} - z^i)(z^i - z^{i-1})$,

$$v^i(\psi) = \frac{\frac{2\mu\lambda}{(z^{i+1} - z^i)(z^i - z^{i-1})}}{\frac{\mu}{(z^i - z^{i-1})} + \frac{\lambda}{(z^{i+1} - z^i)}} v^*(\psi) \tag{8}$$

This definition for $v^i(\psi)$ is proposed by [30] for a comonotone univariate interpolation scheme.

Finally the surface between two consecutive contour z^i and z^{i+1} is given by,

$$S^i(\psi, \theta) = (B^i(\theta, \psi), (1 - \theta)z^i + \theta z^{i+1}) \tag{9}$$

Now the surface between z^1 and z^n is

$$S(\psi, \theta) = \{S^i(\psi, \theta);\ \ i = 1, ..., n - 1,\ \ 0 \leqslant \psi, \theta \leqslant 1\} \tag{10}$$

Boundary Extraction and Corner Detection

To construct the parietal bone fracture, we will initially determined the boundary of each CT scan image using mathematical morphology. The mathematical morphology is defined as $\beta(A) = A - (A \Theta B)$. In this equation A represents the set of all black pixels, B represents 3×3 structured elements, $\beta(A)$ is the boundary set of A, – and Θ represents the difference and erosion operator. To divide the boundary in smaller segments, we use the corner points. Sarfarz et al method [31] is employed to find the corner points.

Parameterization

This manuscript employs the chord length parametrization to find the values of θ_i corresponding to D_i, where D_i represents the data points of each segments.

$$\begin{cases} \theta_0 = 0, \\ \theta_k = \frac{\sum_{i=1}^{k} |D_i - D_{i+1}|}{\sum_{i=1}^{n} |D_i - D_{i+1}|} \quad 1 \leq k \leq n - 1, \\ \theta_n = 1. \end{cases} \tag{11}$$

Normalized Mean Squares Error

$$E^2 = \frac{\sum |s_i(\theta) - D_i|^2}{\sum |D_i|^2}. \tag{12}$$

D_i are the data points of each segments and θ is parameterized by chord length. We will find the free parameters a_i, b_i *and* λ_i in proposed interpolant by minimizing the cost function. Genetic Algorithm (GA) defined in [28] is used to find the a_i, b_i *and* λ_i respectively.

Graphical User Interface(GUI)

GUI consists of one or more windows having control, these are called components. GUI is utilized to perform the interactive tasks and display it graphically. GUI facilitates the users in completion of different tasks. Users are not required to learn the basic programming of each component. GUI consist of start and stop button, panel, scroll bar, push button and boxes etc.

GUI with its individual controls has a executable MATLAB code known as callbacks. The implementation of each callback is activated by a particular user action such as clicking a mouse button, pressing a screen button, typing a string or a numeric value, selecting a menu item, or passing the cursor over to a component. The GUI then reacts to these events. In this manuscript, GUI is used to construct and control the curves of the fractured segment of the parietal bone. The input for curve construction is missing part end points.

Proposed Algorithm

This section simplifies the algorithm for craniofacial fracture reconstruction.

Input: CT scan image in Dicom format.

Output: Constructed 3D craniofacial fracture.

1. Read image as in Fig 7.
2. Boundary extraction Fig 8(c)
3. Corner points detection to make segments of curve Fig 8(d)
4. GC^1 rational Ball curve is used to fit each segment. The unknown parameters a_i, b_i and λ_i in Eq (2) are optimized using Genetic Algorithm Fig 8(d)
5. Step 4 is repeated until a desired solution is obtained
6. Fracture part curves reconstruction for each CT scan slice as in Figs 9 and 10
7. Using GUI for the construction of curves as in Fig 11

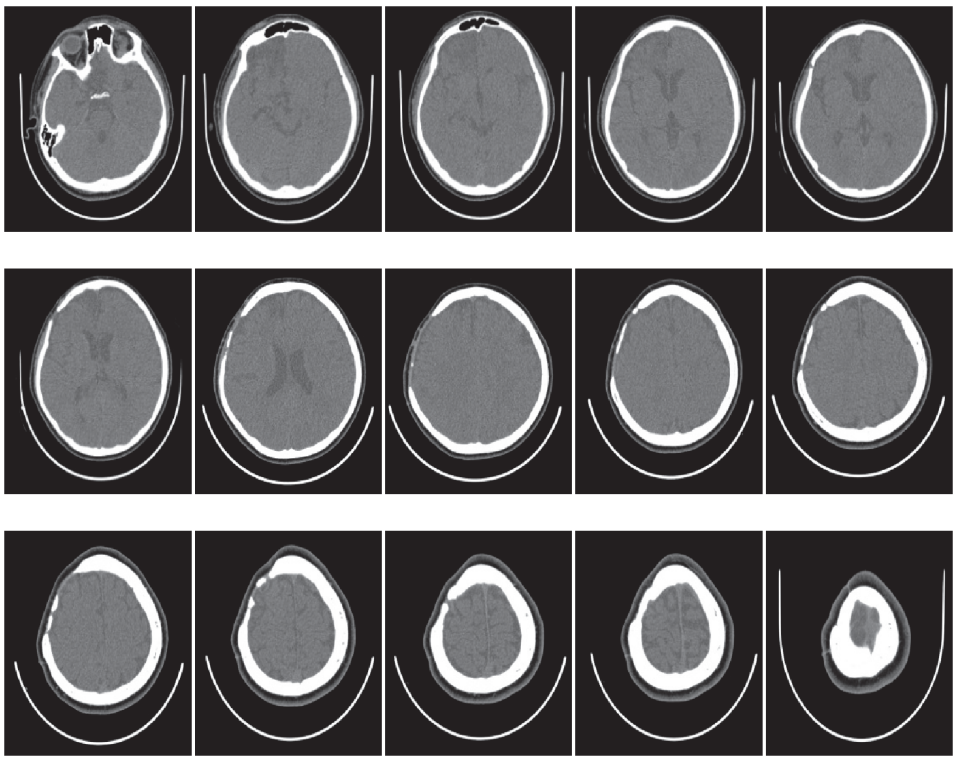

Fig 7. Given CT scanned images of patient with parietal bone fracture.

doi:10.1371/journal.pone.0149921.g007

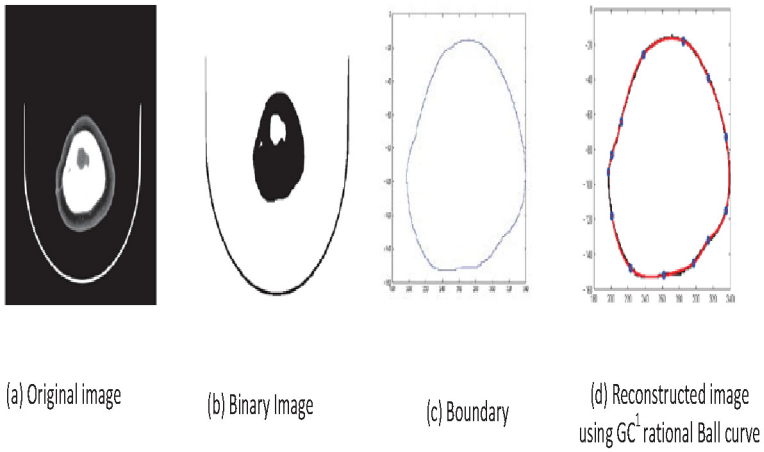

Fig 8. Reconstructed image of CT scan of Dicom slice 178.

doi:10.1371/journal.pone.0149921.g008

8. Conversion of 2D CT scan data into 3D form as in Fig 12
9. Construction of 3D craniofacial fracture using proposed method as in Figs 13 and 14.

In step 4 we reconstruct the boundary curve of a full skull using our proposed method. The genetic algorithm (GA) is used to optimize the free parameters. Normalized mean squares error is used as a cost function in GA and will be repeated until we get the best possible values of free parameters for boundary curve construction as shown in Fig 8(d). The process of optimization terminates when the error is less or equals to 10^{-2} for the desired solution. In Fig 8 (d), reconstructed boundary curve is represented in red, while the original boundary curve is in black.

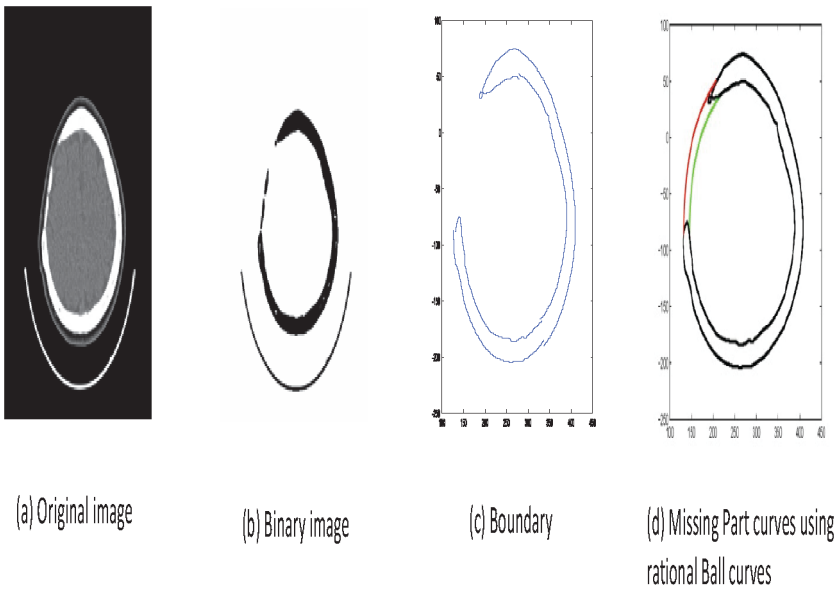

Fig 9. CT scanned data of slice 156.

doi:10.1371/journal.pone.0149921.g009

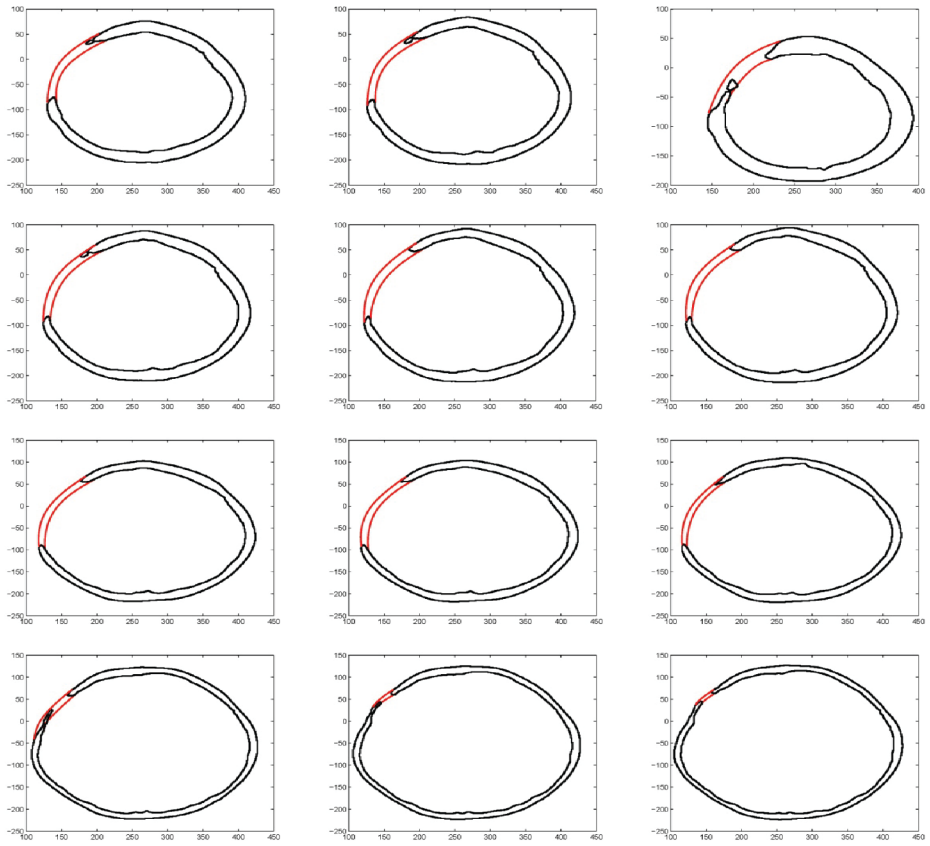

Fig 10. Reconstructed missing part curves for different CT scanned slices.

doi:10.1371/journal.pone.0149921.g010

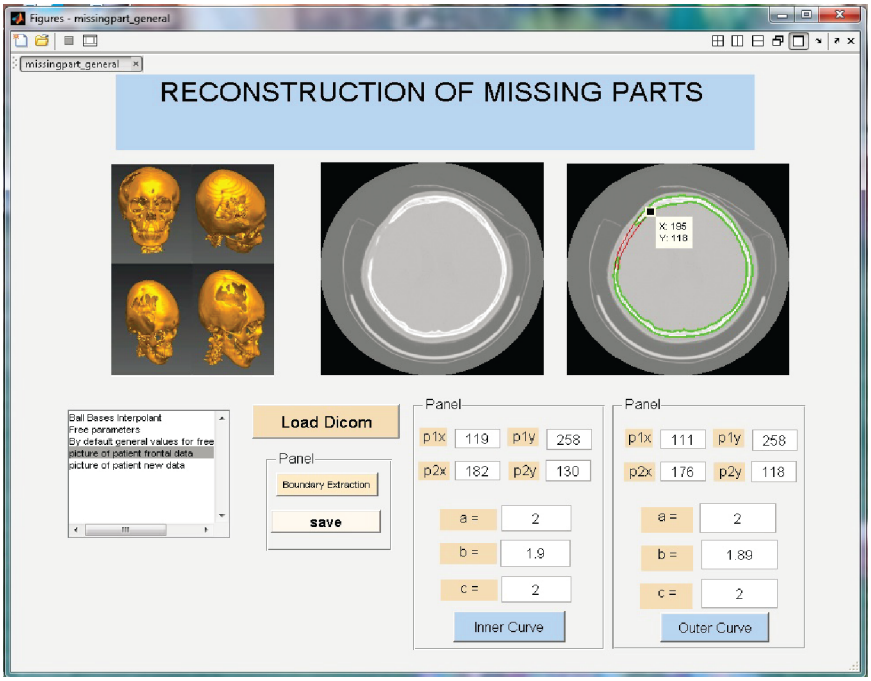

Fig 11. GUI display of craniofacial reconstruction.

doi:10.1371/journal.pone.0149921.g011

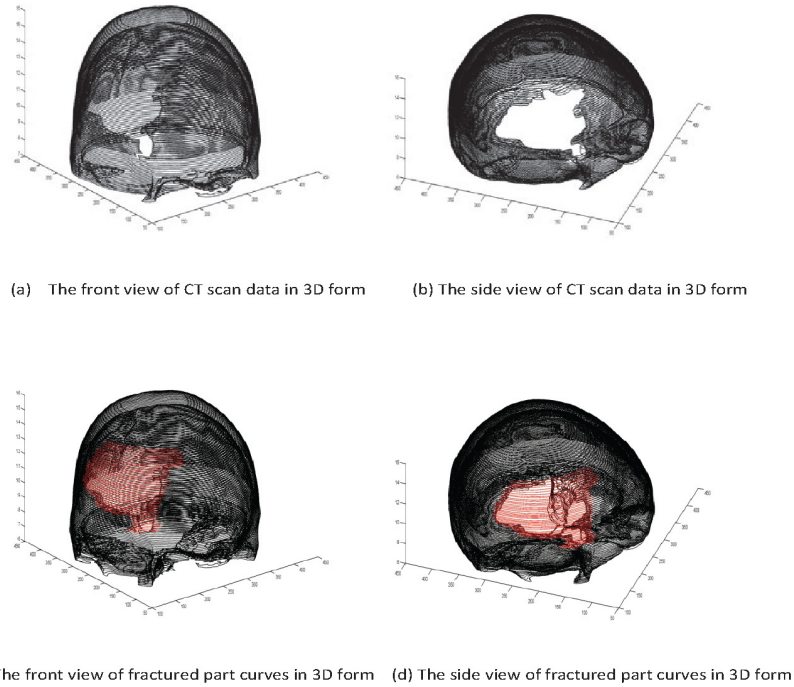

Fig 12. CT scan data in 3D format.

doi:10.1371/journal.pone.0149921.g012

Case study: 3D Craniofacial Fracture Reconstruction

This section illustrates an example of application of the proposed algorithm. The given 2D CT scan Dicom data are in slices as in Fig 7. First, we constructed the boundary curves of complete skull using rational cubic Ball with GC^1 continuity at each knot as shown in Fig 8. Then, we have constructed the inner and outer curves of fractured part for all CT scan slices. Fig 9(a) is the original CT scan of slice 156. For the construction of fractured part, initially, we converted the original image to binary form as shown in Fig 9(b), then, using mathematical morphology, we extracted the boundary of skull as shown in Fig 9(c). Fig 9(d) represents the reconstructed inner and outer curves of fractured part using rational Ball curves. A least square method has been used to evaluate the intermediate control points of a rational Ball curve. The first and last control points of a rational Ball curve will be the starting and end point of the fractured part. The curves can be changed or alter using free parameters defined in Eq (6). Fig 10 shows the construction of fractured part curves of different slices. Fig 11 is the display of Graphical user interface (GUI) which helps in constructing the fractured curves. Next step is to convert the CT scan data and reconstructed fracture curves in 3D form taking equidistant z component as shown in Fig 12. Fig 12(a) and 12(b) are front and side view of CT scan data in 3D form respectively, similarly Fig 12(c) and 12(d) represent the front and side view of 3D CT scan data with fractured part curves respectively. Figs 13 and 14 represent the front and side view of constructed 3D parietal bone fracture using proposed contour blending function.

The Human Research Ethics Committee, Universiti Sains Malaysia, approved the study. Data were collected from archived images of patients from the Picture Archiving and Communication System (PACS) server at the Radiology Department, Hospital Universiti Sains Malaysia. The patients had undergone decompressive craniectomy surgery between May 2009 and December 2014 at the Hospital Universiti Sains Malaysia, Kubang Kerian, Kelantan Malaysia. The medical images were anonymized and the researchers had no access to patients' information.

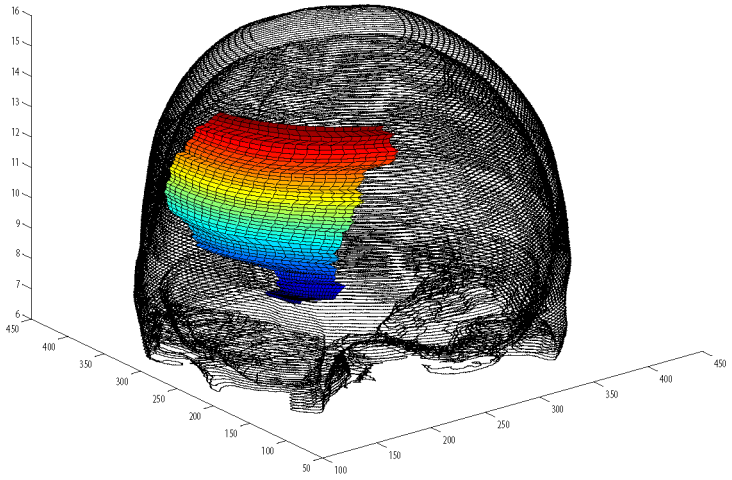

Fig 13. The front view of reconstructed 3D craniofacial fracture.

doi:10.1371/journal.pone.0149921.g013

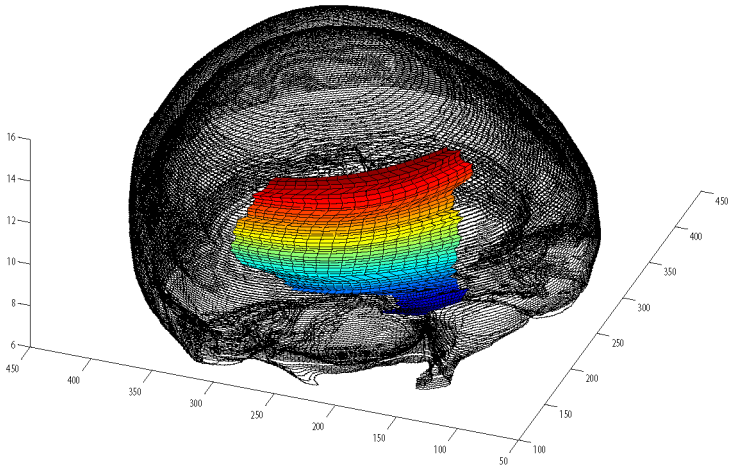

Fig 14. The side view of reconstructed 3D craniofacial fracture.

doi:10.1371/journal.pone.0149921.g014

Conclusion

Contours blending function have been used to construct the 3D surface. A patient with parietal bone fracture have been discussed as a case study to show its applicability. Fracture part curves of each contour is constructed in 2D form using GC^1 rational Ball curves, since the given Dicom data are in 2D form. Then we convert each 2D contour into 3D form taking equidistant z component. The free parameters in proposed interpolant are optimized using Genetic Algorithm. The proposed method will provide the custom made implant for every individual patient. It is also time saving as the surgeon can perform the task of designing the implant geometry without the help of technicians and any other external help. It also reduces the incidence of infection. Proposed method is user friendly due to the presence of GUI.

Acknowledgments

The authors would like to acknowledge Dr Hassan Iqbal's (Resident Oral and Maxillofacial Surgery in Pakistan) input in reading, editing this article and supporting us in elaborating it.

Author Contributions

Conceived and designed the experiments: AM ARMP. Performed the experiments: AM. Analyzed the data: AM ARMP ZRY. Contributed reagents/materials/analysis tools: ZRY AM. Wrote the paper: AM ARMP. Carried out coding: AM ZRY. Wrote and designed the article: ARMP.

References

1. Muller A, Krishnan KG, Uhl E, Mast G. The application of rapid prototyping techniques in cranial reconstruction and pre operative planning in neurosurgery. Journal of Craniofacial Surgery. 2003; 14(6): 899–914. PMID: 14600634
2. Sauret V, Linney A, Richards R. Computer assisted surgery: the use of digital images in enabling computerized design and manufacture of titanium implants. Imaging. 2002; 14(6): 464–471. doi: 10.1259/img.14.6.140464
3. Min Kj, Dean D. Highly accurate CAD tools for cranial implants. In Medical Image Computing and Computer-Assisted Intervention-MICCAI. 2003; Springer: 99–107.
4. Wu T, Engelhardt M, Fieten L, Popovic A, Radermacher K. Anatomically constrained deformation for design of cranial implant: methodology and validation, in. Medical Image Computing and Computer-Assisted 270 Intervention–MICCAI 2006; Springer: 9–16.
5. Wuyang S, MingQuan Z, Qingqiong D, Zhongke W, Fuqing D. 3D craniofacial reconstruction using reference skull-face database, in. Image and Vision Computing New Zealand (IVCNZ). 2010 25th International Conference of, IEEE. 2010; 1–7.
6. Vandermeulen D, Claes P, Loeckx D, Greef DS, Willems G. Computerized craniofacial reconstruction using CT-derived implicit surface representations. Forensic Science International 2006; 159: S164–S174. doi: 10.1016/j.forsciint.2006.02.036 PMID: 16542805
7. Park H, Lee JH. B-spline curve fitting based on adaptive curve refinement using dominant points. Computer-Aided Design. 2007; 39: 439–451. doi: 10.1016/j.cad.2006.12.006
8. Bhatt AD, Warkhedkar RM. Reverse engineering of human body: a B-spline based heterogeneous modeling approach. Computer-Aided Design and Applications. 2008; 5: 194–208. doi: 10.3722/cadaps.2008.194-208
9. Yoshimoto F, Harada T, Yoshimoto Y. Data fitting with a spline using a real-coded genetic algorithm. Computer-Aided Design. 2003; 35: 751–760. doi: 10.1016/S0010-4485(03)00006-X
10. Magnenat TN, Cordier F. Construction of a human topological model from medical data. Information Technology in Biomedicine, IEEE Transactions on. 2000; 4: 137–143. doi: 10.1109/4233.845206
11. Lian Q, Li DC, Tang YP, Zhang YR. Computer modeling approach for a novel internal architecture of artificial bone. Computer-Aided Design. 2006; 38: 507–514. doi: 10.1016/j.cad.2005.12.001
12. Kou X, Tan S. Heterogeneous object modeling: A review. Computer-Aided Design. 2007; 39: 284–301. doi: 10.1016/j.cad.2006.12.007
13. Fang Z. Image-guided modeling, fabrication and micromechanical analysis of bone and heterogeneous structure. Ph.D. thesis, Drexel University 2005.
14. Pimenta S, Tavares JM, Jorge RN, Alexandre F, Mascarenhas T, El Sayed R. Reconstruction of 3d models from medical images: Application to female pelvic organs. cal. 2006; 1(3).
15. Alexandre F, Mascarenhas T, Jorge RN, Parente MP, Fernandes AA, Tavares JMR et al. 3D reconstruction of pelvic floor for numerical simulation purpose. VIPimage 2008.
16. Ma Z, Jorge RN, Mascarenhas T, Tavares JMR. A level set based algorithm to reconstruct the urinary bladder from multiple views. Medical engineering and physics. 2013; 35(12): 1819–1824. doi: 10.1016/j.medengphy.2013.05.002 PMID: 23726217
17. Ma Z, Jorge RNM, Mascarenhas T, Tavares JMR. Segmentation of female pelvic cavity in axial T 2 weighted MR images towards the 3D reconstruction. International journal for numerical methods in biomedical engineering. 2012; 28(6–7): 714–726. doi: 10.1002/cnm.2463 PMID: 25364847
18. Moura DC, Boisvert J, Barbosa JG, Tavares J. Fast 3D reconstruction of the spine using user-defined splines and a statistical articulated model. Lecture Notes in Computer Science (LNCS). 2009.
19. Moura DC, Boisvert J, Barbosa JG, Labelle H, Tavares JMR. Fast 3D reconstruction of the spine from biplanar radiographs using a deformable articulated model. Medical engineering and physics. 2011; 33 (8): 924–933. doi: 10.1016/j.medengphy.2011.03.007 PMID: 21481628

20. Ma Z, Tavares JMR, Jorge RN, Mascarenhas T. A review of algorithms for medical image segmentation and their applications to the female pelvic cavity. Computer Methods in Biomechanics and Biomedical Engineering. 2010; 13(2): 235–246. doi: 10.1080/10255840903131878 PMID: 19657801

21. Ma Z, Tavares JMR, Jorge RMN. A Review on the Current Segmentation Algorithms for Medical Images. In IMAGAPP 2009-Proceedings of the First International Conference on Computer Imaging Theory and Applications, Lisboa, Portugal. 2009; February 5–8: 135–140.

22. Cavalcanti MGP, Rocha SS, Vannier MW. Craniofacial measurements based on 3D-CT volume rendering: implications for clinical applications. Dentomaxillofacial Radiology. 2014.

23. Winslow BD, Shao H, Stewart RJ, Tresco PA. Biocompatibility of adhesive complex coacervates modeled after the sandcastle glue of Phragmatopoma californica for craniofacial reconstruction. Biomaterials. 2010; 31(36): 9373–9381. doi: 10.1016/j.biomaterials.2010.07.078 PMID: 20950851

24. Ball AA. CONSURF. Part one: introduction of the conic lofting tile. Computer-Aided Design. 1974; 6: 243–249. doi: 10.1016/0010-4485(74)90009-8

25. Said H. A generalized Ball curve and its recursive algorithm. ACM Transactions on Graphics (TOG). 1989; 8: 360–371. doi: 10.1145/77269.77275

26. Majeed A, Piah ARM. Image reconstruction using rational Ball interpolant and genetic algorithm. Applied Mathematical Sciences. 2014; 8: 3683–3692.

27. Piah ARM, Unsworth K. Improved sufficient conditions for monotonic piecewise rational quartic interpolation. Sains Malaysiana. 2011; 40: 1173–1178.

28. Majeed A, Mt Piah AR, Gobithaasan RU, Yahya ZR. Craniofacial Reconstruction Using Rational Cubic Ball Curves. PLoS ONE. 2015; 10(4): e0122854. doi: 10.1371/journal.pone.0122854 PMID: 25880632

29. Goodman TNT, Ong BH, Unsworth K. A new algorithm for the reconstruction of 3D objects from cross sections. Proceedings 5th ASEE International Conference ECGDG, Melbourne, Australia. 1992.

30. Butland J. A method of interpolating reasonable shaped curves through any data. In proc. Computer Graphics 80,Middlesex,UK. 1980; 409–422.

31. Sarfraz M, Masood A, Asim M. A new approach to corner detection. In: Computer Vision and Graphics, Springer. 2006; 528–533.